Am J Physiol Heart Circ Physiol 296: H1766–H1773, 2009.
First published April 10, 2009; doi:10.1152/ajpheart.00120.2009.

Active stiffening of mitral valve leaflets in the beating heart

Akinobu Itoh,[1] Gaurav Krishnamurthy,[1,2] Julia C. Swanson,[1] Daniel B. Ennis,[1] Wolfgang Bothe,[1] Ellen Kuhl,[2] Matts Karlsson,[3] Lauren R. Davis,[1] D. Craig Miller,[1] and Neil B. Ingels, Jr.[1,4]

[1]*Department of Cardiothoracic Surgery, School of Medicine, and* [2]*Department of Mechanical Engineering, Stanford University, Stanford, California;* [4]*Department of Cardiovascular Physiology and Biophysics, Research Institute of The Palo Alto Medical Foundation, Palo Alto, California; and* [3]*Department of Management and Engineering, Linköping University, Linköping, Sweden*

Submitted 4 February 2009; accepted in final form 3 April 2009

Itoh A, Krishnamurthy G, Swanson JC, Ennis DB, Bothe W, Kuhl E, Karlsson M, Davis LR, Miller DC, Ingels NB Jr. Active stiffening of mitral valve leaflets in the beating heart. *Am J Physiol Heart Circ Physiol* 296: H1766–H1773, 2009. First published April 10, 2009; doi:10.1152/ajpheart.00120.2009.—The anterior leaflet of the mitral valve (MV), viewed traditionally as a passive membrane, is shown to be a highly active structure in the beating heart. Two types of leaflet contractile activity are demonstrated: *1*) a brief twitch at the beginning of each beat (reflecting contraction of myocytes in the leaflet in communication with and excited by left atrial muscle) that is relaxed by midsystole and whose contractile activity is eliminated with β-receptor blockade and *2*) sustained tone during isovolumic relaxation, insensitive to β-blockade, but doubled by stimulation of the neurally rich region of aortic-mitral continuity. These findings raise the possibility that these leaflets are neurally controlled tissues, with potentially adaptive capabilities to meet the changing physiological demands on the heart. They also provide a basis for a permanent paradigm shift from one viewing the leaflets as passive flaps to one viewing them as active tissues whose complex function and dysfunction must be taken into account when considering not only therapeutic approaches to MV disease, but even the definitions of MV disease itself.

anterior mitral valve leaflet; finite-element analysis; elastic modulus; mitral leaflet contractile tissue; electrical stimulation; β-receptor blockade

MITRAL VALVE (MV) disease afflicts millions worldwide. Medical and surgical therapies for this disease have traditionally assumed that the valve leaflets, the key components of the valve, are passive flaps (46). However, muscle fibers (2, 6, 11, 12, 18, 25, 30–32, 34, 39, 41, 47, 48), blood vessels (6, 8, 11, 24, 26, 37, 39), and nerves (1, 6–13, 18–20, 26, 29, 35, 36, 39, 43–45) have been recognized in the MV leaflets of animals and humans since the 19th century, and the physiological function of these entities, along with other contractile elements in the leaflets, such as smooth muscle (8, 18, 26, 47) and valvular interstitial cells (VICs) (4, 13, 18, 23, 26, 28, 38, 40), is not understood.

MV leaflets have extensive passive collagen fiber networks (5, 11, 12, 15, 18), and the stress-strain relationship of isolated leaflets (3, 14, 22, 27) is consistent with the material properties of passive collagen fibers. Our recent study (21), however, suggested that leaflet stiffness in the beating heart (slope of the leaflet stress-strain curve) was much greater than that of passive tissue, and studies of freshly isolated, oxygenated, stimulated leaflets in myographs (39) and in open hearts on cardiopulmonary bypass (CBP) (7, 32) have suggested that the mechanical properties of MV leaflets may be altered actively. Two important hypotheses have been advanced regarding this activity (46). *1*) Contractile element force development within the leaflets, in response to leaflet excitation (7, 12, 32, 33, 48), provides modulation of leaflet tone to adapt to changes in left ventricular (LV) pressure (LVP) load on the closed valve (33, 49). A key prediction of this hypothesis is that excitation can vary leaflet stiffness in the closed valve. *2*) Leaflet excitation develops a brief twitch contraction to aid valve closure (7, 32, 33, 41). A key prediction of this hypothesis is that leaflet stiffness is transiently increased during valve closure. In the present study, we provide the first tests of these hypotheses by measuring instantaneous leaflet stiffness during isovolumic contraction (IVC) and isovolumic relaxation (IVR) in the beating ovine heart.

Leaflet circumferential and radial stiffness moduli (E_{circ} and E_{rad}, respectively) during IVC and IVR were obtained from inverse finite-element analyses employing transleaflet pressures from left atrial (LA) pressure (LAP) and LVP transducers, along with instantaneous four-dimensional leaflet, annular, and chordal geometry acquired from biplane radiography of markers sewn to the components of the ovine MV. These values were obtained before (CTRL_ESML) and after reversible blockade of β-receptors with intravenous esmolol (ESML) and before (CTRL_STIM) and after stimulation of the region of aortic-mitral continuity (STIM) with subthreshold electrical pulses.

MATERIALS AND METHODS

Experimental animals. We previously reported baseline leaflet E_{circ} and E_{rad} during IVR in a cohort of 17 sheep (21). By protocol, after we acquired these initial baseline data, we conducted two intervention studies (ESML and STIM), with each intervention preceded by its own control (CTRL_ESML and CTRL_STIM). We report here the leaflet elastic modulus response to these interventions (circumferential and radial; now including IVC and IVR) from technically successful experiments in 10 of these 17 animals. To encourage additional analyses of these data, all marker coordinate and pressure data from these experiments are available on request.

All animals received humane care in compliance with the "Principles of Laboratory Animal Care" formulated by the National Society for Medical Research and also in compliance with the National Institutes of Health *Guide for the Care and Use of Laboratory Animals* (NIH Publication No. 85-23, Revised 1985). This study was approved by the Stanford Medical Center Laboratory Research Animal Review Committee, which is accredited by the Association for Assessment and Accreditation of Laboratory Animal Care International, and was conducted according to Stanford University policy.

Address for reprint requests and other correspondence: N. B. Ingels, Jr., Dept. of Cardiovascular Physiology & Biophysics, Research Institute, Palo Alto Medical Foundation, 795 El Camino Real (AMES Bldg.), Palo Alto, CA 94301 (e-mail: ingels@stanford.edu).

Surgical preparation. The sheep (54 ± 8 kg) were premedicated with ketamine (25 mg/kg im) for venous and arterial catheter placement, anesthetized with inhalational isoflurane (1.0–2.5%), intubated, and mechanically ventilated. Once normal cardiac function and valve competency were confirmed with epicardial echocardiography through a left thoracotomy, 13 miniature radiopaque tantalum markers were surgically implanted into the subepicardium to silhouette the LV chamber along four equally spaced longitudinal meridians (ventricular markers, Fig. 1*A*). On CPB, a total of 35 radiopaque tantalum markers were sewn to the following sites: 1 at the tip of each papillary muscle [anterior and posterior papillary muscle (APM and PPM), Fig. 1*A*], 16 around the mitral annulus (annular markers, Fig. 1*A*), 16 on the atrial aspect of the anterior MV leaflet [7 on the MV leaflet edge (*markers 1–7*, Fig. 1*B*) and 9 on the leaflet belly (*markers 8–16*, Fig. 1*B*)], and 1 on the central edge of the middle scallop of the posterior MV leaflet (Fig. 1*A*). A single tantalum loop (0.6 mm ID, 1.1 mm OD, 3.2 mg each) was used for each leaflet marker (Fig. 1*C*). After marker implantation, a pacing wire electrode was placed in the region of aortic-mitral continuity (near *marker 20*, STIM, Fig. 1*B*) and exteriorized. The animals were weaned from CPB, and a micromanometer pressure transducer (model PA4.5-X6, Konigsberg Instruments, Pasadena, CA) was placed in the LV chamber through the LA and exteriorized.

Data acquisition. The animals were transferred to the experimental catheterization laboratory and placed in the right lateral decubitus position for acquisition of data under open-chest conditions. Two micromanometer pressure transducers (model MPC-500, Millar Instruments, Houston, TX) were calibrated and introduced via the carotid artery to measure LVP and aortic pressure (AoP) immediately distal to the aortic valve. The Konigsberg pressure transducer was calibrated (by linear regression of Millar and Konigsberg signals) against the two Millar pressure transducers while all transducers were in the LV, then the Konigsberg was pulled back into the LA for measurement of LAP.

Videofluoroscopic images (60 frames/s) of all radiopaque markers were acquired in multiple-beat runs using a biplane videofluoroscopy system (Philips Medical Systems, Pleasanton, CA) with the heart in normal sinus rhythm and ventilation transiently arrested at end expiration. These images were obtained before (CTRL_ESML) and after (ESML) β-blockade with esmolol (10–25 mg bolus to achieve ~15% reduction in LVP) and then before (CTRL_STIM) and after (STIM) subthreshold pacing via the pacing electrode for ~10 s (1–3 mA, 320/min). Marker coordinates from each view were then merged to yield the three-dimensional coordinates of the centroid of each marker in each frame. LVP, LAP, AoP, and ECG voltage signals were digitally recorded simultaneously during marker data acquisition and synchronized with the images. After data acquisition, the animals were euthanized, and the hearts were excised. Ex vivo photographs of the MV and subvalvular apparatus were used to identify the chordae tendineae insertion points on the MV leaflet.

Hemodynamics and cardiac cycle timing. Three consecutive beats in sinus rhythm were selected for analysis for each of the four runs (CTRL_ESML, ESML, CTRL_STIM, and STIM) in each heart. For each of these beats, the valve closure time point (t_1) was defined as the frame when the distance between *marker 4* on the anterior leaflet and its counterpart on the central posterior leaflet initially fell to a stable minimum (Fig. 1*D*, lower left red dot) and LVP and LAP at that time were noted (LVP_1 and LAP_1). The end IVC time point (t_2, Fig. 1*D*, upper left red dot) was defined from the AoP deflection, and LVP and LAP at that time were noted (LVP_2 and LAP_2). The frame during IVR when LVP most closely matched LVP_1 (Fig. 1*D*, lower right blue dot) was defined as t_3, with pressures LVP_3 and LAP_3. The frame during IVR when LVP most closely matched LVP_2 (Fig. 1*D*, upper right blue dot) was defined as t_4, with pressures LVP_4 and LAP_4. Figure 1*D*

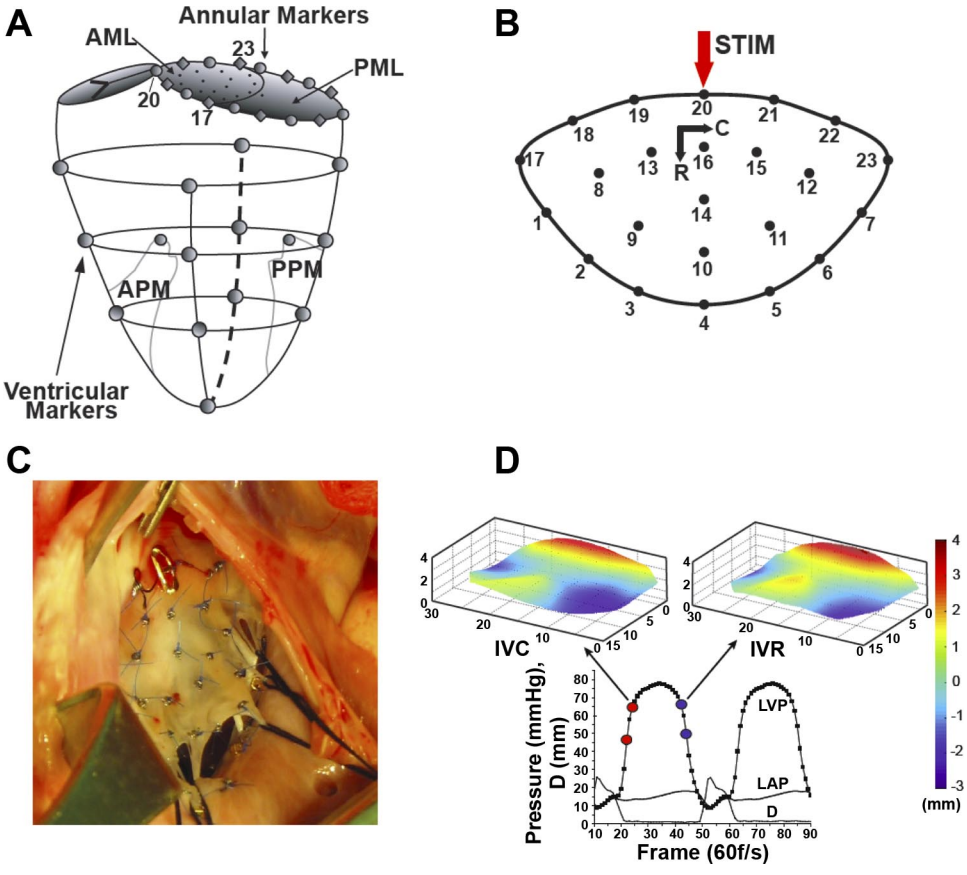

Fig. 1. *A*: radiopaque marker sites on left ventricle (LV), mitral annulus, and leaflets. AML and PML, anterior and posterior mitral valve (MV) leaflet; APM and PPM, anterior and posterior papillary muscle. *B*: radiopaque marker sites on the MV anterior leaflet, with circumferential (*C*) and radial (*R*) axes and subthreshold electrical pulse stimulation site (STIM). *C*: intraoperative photograph of markers sewn to the MV anterior leaflet. *D*: representative LV pressure (LVP), left atrial pressure (LAP), and interleaflet distance (*D*) data showing LVP interval during which isovolumic contraction (IVC) stiffness is measured (red dots) and anterior leaflet shape at the end of IVC (*top left*) and pressure-matched LVP interval during which isovolumic relaxation (IVR) stiffness is measured (blue dots) and anterior leaflet shape at the beginning of IVR (*top right*). Leaflet vertical dimension is color-coded from −3 to +4 mm to illustrate leaflet shape.

shows leaflet geometry at the t_2 and t_4 matched LVPs for a representative beat in this study.

Finite-element analysis. Finite-element models of the anterior MV leaflet were individually developed for IVC and IVR intervals for each of the 30 beats analyzed using Hypermesh version 8.0 SR 1 (Altair Hyperworks, Troy, MI) to construct the geometry and meshing of the leaflet and Optistruct version 8.0 SR 1 (Altair) as the solver.

The geometry of the anterior leaflet was initially defined by the leaflet marker positions (Fig. 1*B*) at t_1 for IVC and t_3 for IVR. The *x, y,* and *z* coordinate values for each of the leaflet and annular marker positions at these times were entered as points in Hypermesh. Five cubic splines were generated through *1*) *markers 17-1-2-3-4-5-6-7-23*, *2*) *markers 18-8-9-10-11-12-22*, *3*) *markers 19-13-14-15-21*, *4*) *markers 19-16-21*, and *5*) *markers 19-20-21*. These splines were used to generate a bicubic leaflet surface.

For the purpose of defining the MV leaflet material properties, a coordinate system was defined with origin at the center of the 16 markers defining the saddle-shaped annulus at t_1 for IVC and t_3 for IVR. A line from this origin to *marker 20* was defined as the leaflet radial axis (*R*, Fig. 1*B*). The leaflet circumferential axis (*C*, Fig. 1*B*) was defined normal to *R* and in the plane containing *R* and the posterior commissural marker (*marker 23*, Fig. 1, *A* and *B*).

The material model of the leaflet was assumed to be orthotropic linear elastic (MAT8 in Hypermesh), an assumption supported by our analysis (unpublished observations) showing that the stress-strain relationship of these leaflets is linear over the physiological range of pressures in these beating hearts. Two regions (PSHELL in Hypermesh) were used to define the varying thickness of the leaflet with use of thickness data obtained from our histological study of an anterior leaflet from a representative ovine heart. The first defined a region from the annulus to 75% of the leaflet toward the free edge; this region had thickness values that varied linearly from 1.2 mm at the annulus to 0.7 mm 75% toward the leaflet free edge. The second region defined the remaining 25% of the leaflet with a uniform thickness of 0.2 mm.

The bicubic surface fit of the MV leaflet was then meshed with plane-stress quadrilateral shell elements. A typical anterior leaflet was meshed with 2,200 elements, yielding an element size of 0.004 cm^2. This mesh allowed experimental displacements to be matched with $<$5% root-mean-square error for the final material properties obtained.

The strut chordae were defined as ropelike structures undergoing pure tension (MAT1 in Hypermesh). A previously published ex vivo modulus (elastic modulus = 20 N/mm^2, cross sectional area = 0.008 cm^2) was used for the strut chordae (22). Tension-only bar elements (PBARL in Hypermesh) were defined as radiating from the papillary muscle tip marker points (APM and PPM, Fig. 1*A*) to leaflet belly insertion positions as defined from the anatomic photographs.

The boundary conditions were then enforced on the finite-element models. For IVC, (LVP_2-LVP_1) was applied to the ventricular surface of the leaflet and (LAP_2-LAP_1) to the atrial surface. For IVR, (LVP_4-LVP_3) was applied to the ventricular surface and (LAP_4-LAP_3) to the atrial surface. The displacements of the annular markers (*markers 17–23*, Fig. 1*B*), anterior leaflet edge markers (*markers 1–7*, Fig. 1*B*), and papillary tip markers (APM and PPM, Fig. 1*A*) were defined using actual marker data from t_1 to t_2 for IVC and from t_3 to t_4 for IVR.

The Hypermesh finite-element model was then solved for the enforced boundary conditions using Optistruct to obtain the simulated displacements of the leaflet belly markers (*markers 8–16*, Fig. 1*B*).

Inverse finite-element analysis algorithm. The Optistruct solver was interlinked with commercial optimization software, Hyperstudy version 8.0 SR 1 (Altair Hyperworks), to run an inverse finite-element analysis to yield the in vivo material properties of the valve leaflet during IVC and IVR. In this algorithm, the model-simulated displacements of the nine leaflet belly markers (*markers 8–16*, Fig. 1*B*) from each iteration were compared with the actual measured displacements of these nine markers during IVC or IVR to yield an objective function defined as the root-mean-squared displacement difference between measured and actual displacements of the nine leaflet belly markers. Hyperstudy then used a parameter identification algorithm, the method of feasible directions, to minimize the objective function by successive iterative refinement of the material properties (E_{circ} and E_{rad}) in each finite-element simulation until a global minimum was obtained. Leaflet circumferential-radial shear during IVC and IVR proved sufficiently small that E_{circ} and E_{rad} values so obtained were unchanged with inclusion or exclusion of this shear in the parameter identification process.

An absolute convergence value of 0.0001 cm (a relative convergence of 0.01%) typically required 13 ± 3 iterations and 10 ± 2 min for each heartbeat analyzed. The material property values (E_{circ} and E_{rad}) obtained at the end of the parameter identification runs, with the objective function at its global minimum, were interpreted as the in vivo material properties of the anterior MV leaflet belly during IVC and IVR. That is, these material property values, when used in the finite-element model for the anterior leaflet belly under the enforced pressure and geometric boundary conditions, produced, as closely as possible, the same leaflet belly marker displacements measured experimentally during IVC and IVR.

Statistical analysis. Values are group means ± SD. Three-beat averages were used to characterize the data for each animal. Data were compared using one- and two-way repeated-measures ANOVA with Bonferroni's post hoc test (Sigmastat 3.5, Systat Software, San Jose, CA). Statistical significance was set at $P < 0.05$ unless otherwise specified.

RESULTS

Table 1 shows the hemodynamic and annular dimensional response to the ESML and STIM interventions. Relative to

Table 1. *Hemodynamics and annular dimensions*

	CTRL_ESML	ESML	CTRL_STIM	STIM
Heart rate, min^{-1}	88±13	83±11*	84±11*	83±11*
LV ESV, ml	100±16	104±18*	104±17*	104±18*
LV SV, ml	26±6	23±7*	24±6	24±6
LV EDP, mmHg	14±3	15±3	15±3	16±3
LV ESP, mmHg	84±8	71±12*	74±9*	71±9*
S-L dimension at ES, cm	2.5±0.2	2.6±0.2	2.5±0.2	2.5±0.2
C-C dimension at ES, cm	3.5±0.3	3.6±0.3*	3.6±0.3*	3.6±0.3*
Total annular perimeter at ES, cm	10.8±0.7	11.0±0.7*	11.1±0.7	11.0±0.7
Mitral annular area at ES, cm^2	8.1±1.1	8.5±1.0*	8.6±1.3*	8.5±1.3*

Values are group means ± SD (n = 10). LV, left ventricular; ESV, end-systolic volume; SV, stroke volume; EDP, end-diastolic pressure; ESP, end-systolic pressure; S-L, septal-lateral; C-C, commissure-commissure; ES, end systole. Control data (CTRL_ESML and CTRL_STIM) were obtained immediately before esmolol (ESML) and subthreshold electrical pulse stimulation (STIM) interventions, respectively. *$P \leq 0.001$ vs. CTRL_ESML [by 1-way repeated-measures ANOVA with Bonferroni's post hoc test (level of significance adjusted to $P < 0.05/4$)].

CTRL_ESML, ESML β-blockade reduced heart rate, stroke volume, and LV end-systolic pressure; increased LV end-systolic volume and mitral annular commissure-commissure and perimeter dimensions and area; but did not change LV end-diastolic pressure. From CTRL_STIM to STIM, these values were unchanged, inasmuch as the STIM pulses were intentionally subthreshold. Differences between CTRL_STIM and CTRL_ESML likely result from CTRL_STIM consistently following CTRL_ESML in the protocol.

Table 2 and Fig. 2 show the responses of leaflet moduli to the ESML and STIM interventions. [To avoid cumbersome triple-subscript notation, we identify modulus variables by column (*A–H*) and row (*1–2*) in Table 2 and Fig. 2 (e.g., *A1* for CTRL_ESML IVC E_{circ}, *H2* for STIM IVR E_{rad}).]

We found that *1*) MV leaflet stiffness is anisotropic, with E_{circ} 2.7–3.3 times greater than E_{rad} under all conditions (mean $A1 = 2.9 \cdot A2$, $B1 = 3.0 \cdot B2$, $C1 = 3.3 \cdot C2$, $D1 = 3.0 \cdot D2$, $E1 = 2.9 \cdot E2$, $F1 = 3.1 \cdot F2$, $G1 = 2.7 \cdot G2$, and $H1 = 2.9 \cdot H2$), *2*) MV leaflet stiffness changes during the cardiac cycle, with control IVC stiffness 1.5–1.7 times greater than control IVR stiffness for E_{circ} and E_{rad} (mean $A1 = 1.5 \cdot B1$, $A2 = 1.6 \cdot B2$, $E1 = 1.6 \cdot F1$, and $E2 = 1.7 \cdot F2$), and the control IVC-IVR stiffness difference was anisotropic, with the circumferential difference two to three times that of the radial difference [$(A1 - B1) = 2.6 \cdot (A2 - B2)$ and $(E1 - F1) = 2.7 \cdot (E2 - F2)$], *3*) ESML had no effect on IVR stiffness ($D1 = B1$ and $D2 = B2$) but reduced IVC stiffness to that of IVR [$(D1 = C1) < A1$ and $(D2 = C2) < A2$], *4*) STIM doubled IVR stiffness from CTRL ($H1 = 1.9 \cdot F1$ and $H2 = 2.0 \cdot F2$) but preserved the anisotropic stiffness ratio ($H1 = 2.9 \cdot H2$), and *5*) STIM increased IVC stiffness in parallel with IVR stiffness [$(G1 - E1) = (H1 - F1)$ and $(G2 - E2) = (H2 - F2)$].

Figure 3, histological sections of an ovine anterior MV leaflet, shows the expected continuity between LA muscle and atrial muscle on the atrial side of the anterior MV leaflet (Fig. 3, *A* and *D*), scattered muscle cells and collagen fibers in the leaflet (Fig. 3, *B* and *C*), and bands of smooth muscle just beneath the atrial and ventricular leaflet surfaces (Fig. 3, *E* and *F*).

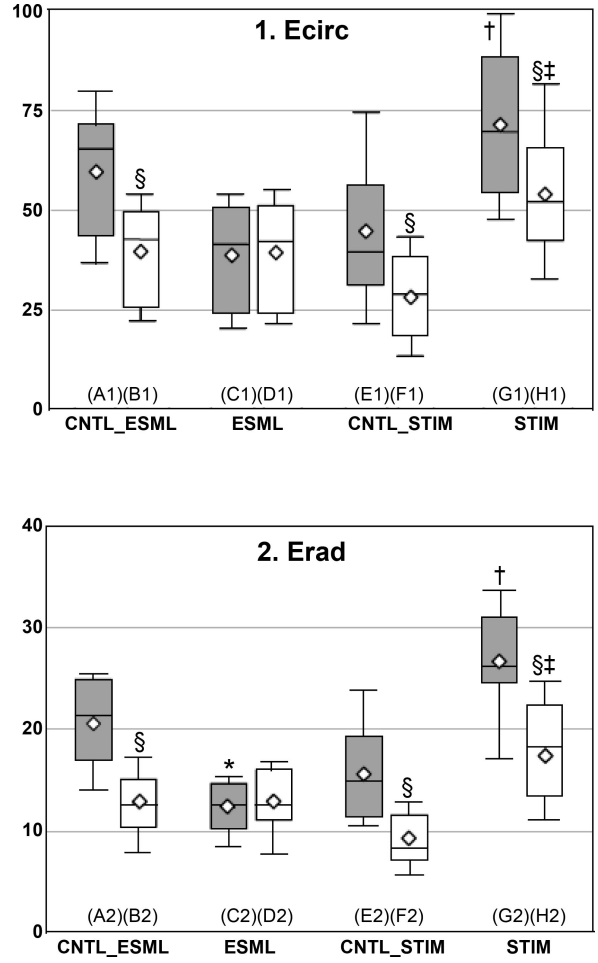

Fig. 2. Leaflet moduli (N/mm^2): circumferential modulus (E_{circ}) and radial modulus (E_{rad}). Control data (CTRL_ESML and CTRL_STIM) were obtained immediately before esmolol (ESML) and subthreshold electrical pulse stimulation (STIM) interventions, respectively. Gray bars, moduli during IVC; open bars, moduli during IVR. Labels below bars link these data to *columns A–H* and *rows 1* and *2* in Table 2. Box plot displays group minimum and maximum values (horizontal lines, *bottom* and *top*), 25th and 75th percentiles (*bottom* and *top* of box), mean (◇), and median (horizontal line within box). Statistically significant differences [$P < 0.001$, by 2-way repeated-measures ANOVA with Bonferroni's post hoc test (with level of significance was adjusted to $P < 0.05/8$)] are as follows: **C* vs. *A*, †*G* vs. *E*, ‡*H* vs. *F*, and §IVR vs. IVC.

DISCUSSION

The results of the present study strongly support both hypotheses tested. We found *1*) an increase in leaflet stiffness of the closed valve during IVR and IVC in response to subthreshold electrical stimulation of the remote, neurally rich region of aortic-mitral continuity and *2*) a transient increase in MV leaflet stiffness during IVC, above IVR values, that is abolished by β-receptor blockade.

Table 2. *Leaflet moduli*

	CTRL_ESML		ESML		CTRL_STIM		STIM	
	IVC (*A*)	IVR (*B*)	IVC (*C*)	IVR (*D*)	IVC (*E*)	IVR (*F*)	IVC (*G*)	IVR (*H*)
E_{circ} (*1*)	60±15	39±12§	39±12*	39±12	44±16	28±11§	72±18†	53±16‡§
E_{rad} (*2*)	21±4	13±3§	12±3*	13±3	15±4	9±3§	27±5†	18±5‡§

Values (means ± SD) are expressed in N/mm^2 ($n = 10$). E_{circ}, circumferential modulus; E_{rad}, radial modulus; IVC, isovolumic contraction; IVR, isovolumic relaxation. Control data (CTRL_ESML and CTRL_STIM) were obtained immediately before esmolol and subthreshold electrical pulse stimulation interventions, respectively. *A–H* are column identifiers, and *1* and *2* are row identifiers. $P < 0.001$ [by 2-way repeated-measures ANOVA with Bonferroni's post hoc test (level of significance adjusted to $P < 0.05/4$)]: **C* vs. *A*; †*G* vs. *E*; ‡*H* vs. *F*; §IVR vs. IVC.

Three force-developing leaflet components are currently known that could account for these stiffening behaviors: leaflet cardiac muscle, leaflet smooth muscle, and VICs.

Leaflet cardiac muscle. The atrialis layer of the anterior MV leaflet contains cardiac muscle cells and well-defined cell bundles, several myofibrils thick, arranged end-to-end and side-to-side, in continuity with LA muscle, surrounded by connective tissue, accompanied by blood vessels and efferent nerves, and tapering in thickness, number, and orientational regularity from annular base to central leaflet, with only slips of muscle near the occlusive margin (2, 6, 11, 12, 18, 30, 39, 47, 48). As shown in Fig. 3, *A* and *D*, this muscle is present at this location in the ovine anterior leaflet. The ultrastructure of this cardiac muscle is similar to that of atrial muscle (12), and, similar to LA muscle, such cells contract with electrical stim-

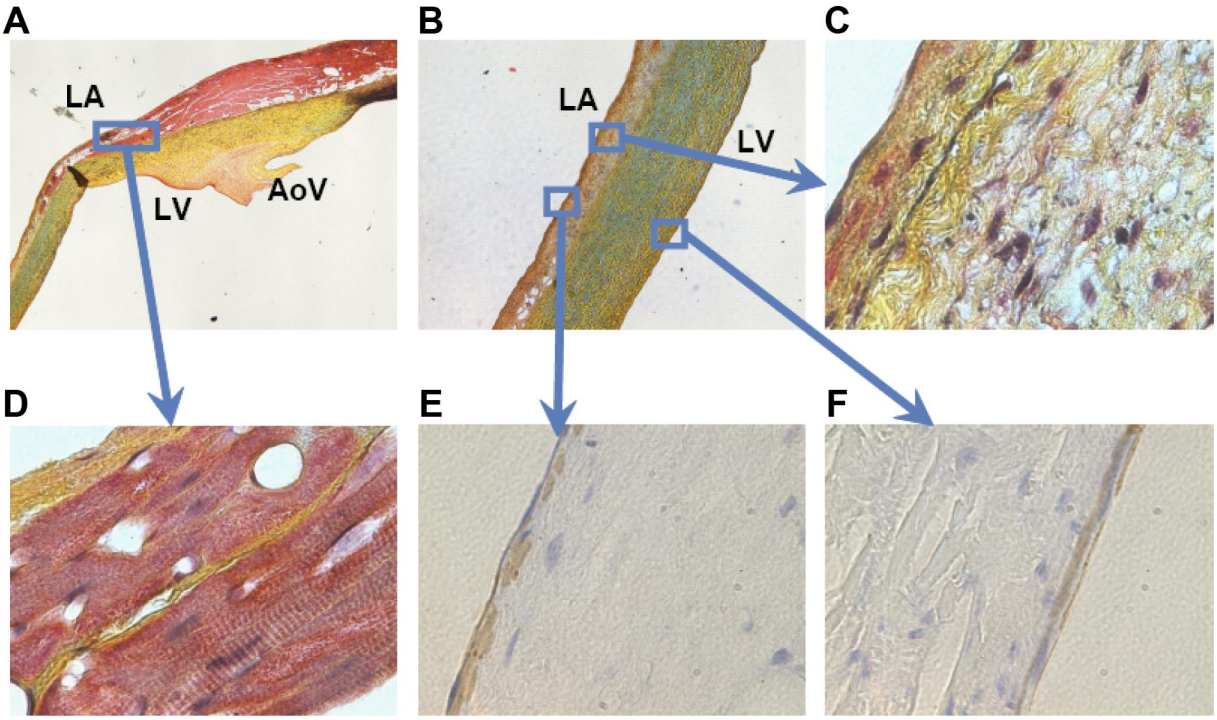

Fig. 3. Muscle and collagen staining of an ovine MV anterior leaflet that was immersed in 10% buffered formalin, dehydrated, and embedded in paraffin wax blocks. LA, left atrial surface; LV, LV surface; AoV, aortic valve. Adjacent radial slices from the middle of the leaflet stained with Silverman-Movat Pentachrome (*A–D*; red = muscle, yellow = collagen, blue = glycosaminoglycans, black = elastin) and for smooth muscle α-actin (*E* and *F*; brown = smooth muscle). Original magnification ×16 (*A* and *B*), ×50 (*C*), and ×1,000 with oil immersion (*D–F*). Isolated smooth muscle cells may also be present throughout the leaflet, although they are not visible at this magnification. Pattern and distribution of structural components that comprise MV leaflets of mammals vary in different species; thus, although there are many similarities, caution must be exercised in extrapolating these results to other species. The extent to which myocytes extend from the annulus into the leaflet, roughly one-third to one-half of the distance from the mitral annulus to the leaflet edge, appears to be a common feature of human anterior MV leaflets (30) and these ovine anterior MV leaflets. Such structural measurements suggest major heterogeneity in leaflet architecture that could significantly affect regional leaflet stiffness.

ulation (12, 39) via propagated depolarization [35-ms stimulus latency, 210-ms refractory period, 6% shortening (39)] and exhibit a positive inotropic response to norepinephrine and tyramine and a negative inotropic response to stimulus frequency (25, 39) and acetylcholine (reversible with atropine) (12, 39).

We propose that this leaflet atrial muscle is responsible for the twitch behavior of the closing valve during IVC, but not the tone behavior of the closed valve during IVR. Previous studies demonstrated that anterior leaflet cardiac muscle is excited with each atrial systole (7, 33) and, similar to atrial myocardium (25), contracts for only ~200 ms after the onset of ventricular systole (32). In isolated tissue, excitation propagates from the LA into the anterior leaflet (12, 48) but spreads more slowly in the leaflet (40–60 ms) than in the atrium (6–10 ms) (12), with force developed for ~200 ms, at most, after transmembrane depolarization of leaflet cardiac muscle (12). However, as shown in Fig. 1*D*, 200 ms (12 frames) corresponds to less than half of ventricular systole in these ovine hearts. Thus, as with LA muscle itself, leaflet cardiac muscle is expected to develop active force during IVC, but it is not expected to contribute to leaflet stiffness during IVR, inasmuch as it is relaxed at that time.

Leaflet smooth muscle. Anterior MV leaflets also contain smooth muscle. The atrialis layer of anterior leaflets contains smooth muscle cells and cell bundles (2–30 cells thick), located in association with blood vessels and elastic sheets and in close proximity to unmyelinated nerve terminals and observed most prominently in proximal and middle regions of the leaflet, but also in the distal third near the leaflet edge (8, 18, 26, 47). As reported by Wit et al. (47), we observed layers of smooth muscle cells just beneath the endocardial cell layers on the atrial and ventricular surfaces of the ovine anterior leaflet (Fig. 3, *E* and *F*). Smooth muscles can also respond rapidly to stimulation, as required in the present STIM study, where stiffness changed within tens of seconds after the onset of electrical stimulation. Thus smooth muscles could provide variable, multibeat leaflet tone that could be observed in the closed valve during IVR, when leaflet atrial muscle is relaxed.

We do not think, however, that smooth muscle per se is responsible for the twitch or tone stiffening observed. Previous studies have shown that the maximum force-developing capability of smooth muscle ranges from 0.003 to 0.87 N/mm^2 (16, 17, 50) and that the elastic modulus of such muscle ranges from 0.008 to 0.36 N/mm^2 (17, 50). Our analysis shows that the maximum force required in the ovine anterior leaflet ranges from 1 to 4 N/mm^2, with E_{circ} and E_{rad} of 5–100 N/mm^2 (Fig. 2). Thus, even if the entire leaflet was composed of smooth muscle, it would be incapable of generating sufficient force or elastic modulus. Smooth muscle is quite sparsely distributed in these leaflets (Fig. 3); thus, although smooth muscle cannot be entirely ruled out as part of a stiffening mechanism, it fails to account for the force and moduli of the leaflet in the beating heart by one to two orders of magnitude.

VICs. Anterior MV leaflets also contain VICs, occupying large portions of the leaflet, particularly the medial and distal regions (4, 13, 18, 23, 38, 40). VICs have characteristics intermediate between fibroblasts and smooth muscle cells (13). They come in close contact with extracellular collagen and may be targets for nearby adrenergic motor nerves, the terminals of which are closely apposed (30–80 nm) (13, 26). VICs have communicating (gap) junctions, so that activity set up in one cell can readily spread to the next cell without significant delay (13). They are contractile: epinephrine and angiotensin II induce very slow, tonic contractions (likely actomyosin-based) in cultured and valvular strips (13, 38). Their collagen synthesis and smooth muscle α-actin content, and hence stiffness, may relate directly to the pressure experienced by the leaflet (28).

The contractile behavior of VICs in vitro, however, is insufficient to account for the rapid increase in stiffness observed in the present STIM study (responses observed within tens of seconds after the onset of electrical stimulation), inasmuch as VICs in vitro exhibit very slow (minutes to hours) force-developing responses to epinephrine or electrical stimuli (13, 38). However, because of their ubiquity and smooth muscle-like behavior and the possibility that VICs in vivo may have a much faster response to stimulation than VICs in vitro, they are good candidates for the stiffness observed during IVR that is increased with STIM.

Conceptual leaflet material model. Figure 4 provides a conceptual model consistent with the material behavior observed in the present in vivo study, as well as the findings from previous ex vivo studies (3, 14, 22, 27). The passive collagen fibers in the leaflet are represented by coiled springs, and the finding that circumferential stiffness is greater than radial stiffness in isolated leaflets (3, 14, 22, 27) results from a model-postulated greater density of circumferentially oriented than radially oriented collagen fibers. Contractile elements (red arrows, possibly VICs), in close proximity to these collagen fibers (40) and developing force in vivo, but not ex vivo, greatly increase all collagen spring constants in vivo relative to in vitro. Thus, as we reported recently (21), IVR leaflet elastic moduli are increased in vivo by orders of magnitude from ex vivo values, but the stiffness anisotropy, with circumferential stiffness much greater than radial stiffness, is maintained in the beating heart (Table 2: $B1 = 3 \cdot B2$ and $F1 = 3.1 \cdot F2$). Although circumferential and radial elements are illustrated as independent entities in Fig. 4, they may also be coupled, as discussed by May-Newman and Yin (27) and supported by the parallel circumferential and radial response to the ESML and STIM interventions in the present study.

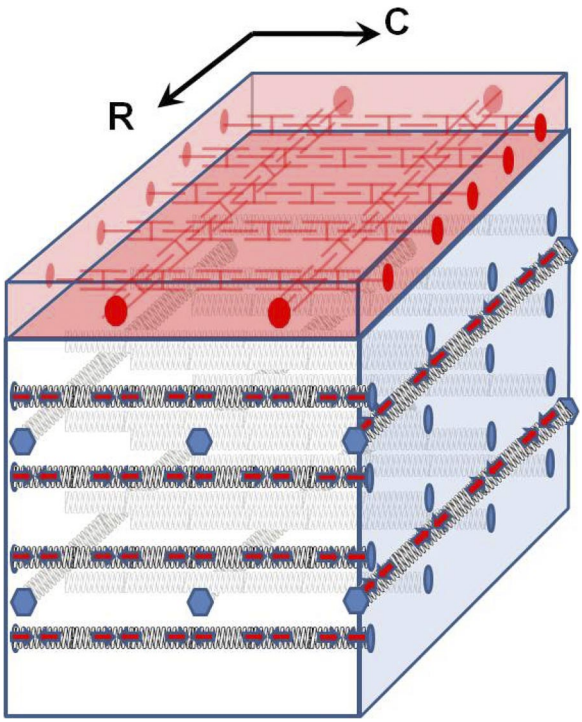

Fig. 4. Conceptual leaflet microstructure. Black springs, collagen; red arrows, valvular interstitial cells; red interdigitating symbols, leaflet atrial muscle.

In this model, the contractile elements (possibly VICs) associated with the collagen fibers provide the more slowly varying leaflet tone that *1*) is unresponsive (or perhaps only very slowly responsive) to β-blockade, *2*) is present during IVC and IVR, *3*) is doubled by STIM (Table 2: $H1 = 1.9 \cdot F1$ and $H2 = 2.0 \cdot F2$), yet *4*) preserves leaflet anisotropy (Table 2: $H1 = 2.9 \cdot H2$). The red entities at the top of Fig. 4 represent leaflet atrial muscle (Fig. 3, *A* and *D*) that is stimulated during each atrial systole, exhibits a brief (<100-ms) twitch response (abolished by β-blockade) during IVC, but is no longer contracting during IVR. In the present study, leaflet atrial muscle increased circumferential and radial leaflet stiffness transiently during IVC relative to IVR by ≥50% (Table 2: $A1 = 1.5 \cdot B1$, $A2 = 1.6 \cdot B2$, $E1 = 1.6 \cdot F1$, and $E2 = 1.7 \cdot F2$). Leaflet muscle was unresponsive to the subthreshold STIM, inasmuch as the stiffness increments (*G1-H1*) and (*E1-F1*) did not differ significantly, nor did (*G2-H2*) and (*E2-F2*); thus the significant increase in IVC stiffness with STIM appears to result from the STIM-induced increase in IVR stiffness alone.

IVC twitch. The anisotropy of the twitch response suggests the presence of two to three times greater force development from leaflet atrial fibers oriented circumferentially than radially during IVC [Table 2: $(A1 - B1) = 2.6 \cdot (A2 - B2)$ and $(E1 - F1) = 2.7 \cdot (E2 - F2)$], as schematically depicted in Fig. 4. This may reflect the unusual structure of leaflet atrial muscle cells that have been observed to form a loose meshwork and interweave with and cross over each other, are attached not only end-to-end, but also side-to-side, and contain myofibrils oriented in many directions (11, 18), yet with a pronounced circumferential orientation. Such a meshwork could briefly augment radial and circumferential leaflet stiffness to prevent ballooning of the cusps during IVC when the valve is suddenly subjected to high LVP. These IVC findings, coupled with the previous demonstration of a transient bending of the anterior leaflet toward the posterior leaflet that can be abolished by ablation of leaflet cardiac muscle in the open heart on CPB (7, 32, 33) and ablation of leaflet cardiac muscle that delays leaflet closure by ~35 ms in the pumping heart (41), support the concept that transient twitch contractions of leaflet atrial muscle aid valve closure.

Neural networks. We do not know whether the electrical pulses in the STIM study were operating directly or by paracrine mechanisms, although we favor the latter, considering the very high rate and subthreshold amplitude of the STIM pulses. There are ample efferent neural networks in the LA subendocardial plexus [the most profusely innervated area of the heart

(29)], annulus, leaflet, chordae, and papillary muscles (1, 6, 8, 10, 12, 18, 26, 43–45) to carry this stimulus from the aortic-mitral continuity into the anterior leaflet. Within the anterior leaflet, however, no myoneural junctions are observed (18, 39), the neuromuscular distance being >50 nm and filled with connective tissue (8, 18); thus contractile myofibers in the leaflet are not directly innervated, and paracrine action is most consistent with our findings. VICs, however, may be directly innervated, inasmuch as Tsumori and Domoto (42) reported that axon terminals make direct contact (<20 nm) with mitral VICs. The pattern of unmyelinated adrenergic fibers in the anterior leaflet is generally paravascular (1), with some terminals in regions devoid of blood vessels and muscle (11, 18) and some in distal leaflet regions closely apposed to VICs (13). These terminals may release ligands that, through paracrine action, modulate the tension of VICs and/or smooth muscle in the leaflet, remote from the stimulus origin. In vitro studies have demonstrated that tyramine (which causes release of endogenous norepinephrine from nerve terminals), as well as acetylcholine, can alter the contractile properties of isolated anterior leaflets (39). In vivo studies of unloaded anterior MV leaflets reveal conformational changes with vagal and stellate ganglion stimulation (7), suggesting a role for the sympathetic and parasympathetic divisions of the autonomic nervous system.

Possible leaflet control system. The fact that these two contractile systems exist in the valve leaflets and that the mechanical properties of both systems can be modified provides provisional support for the concept of an MV leaflet adaptive control system. Our working hypothesis is that mechanoreceptors in the leaflet may monitor leaflet stretch and that leaflet sensory (afferent) nerves transmit this information for local reflex and/or central processing. Anterior leaflets are known to be richly innervated with sensory and motor nerves (1, 19, 20, 36, 43–45) [adrenergic and cholinergic (6, 8–10)], with unmyelinated axons (18) and thick myelinated fibers (8, 18, 29, 43–45) (which may serve as mechanoreceptors) coursing through the atrial subendocardial plexus. Leaflet contractile elements could thus be appropriately activated via motor nerves to maintain constant anterior MV leaflet shape and position immediately before and during valve closure over the wide range of LV operating pressures and volumes. The resulting relatively constant anterior leaflet shape and position in the nearly closed and closed valve could *1*) prevent major leaflet mechanical closing shock with each beat, inasmuch as the leaflets are already very nearly apposed immediately before the sudden pressure rise with ventricular systole, 2) allow the other leaflets of the valve to coapt with a relatively stationary, rather than moving, anterior leaflet target, which could precisely stabilize the precoaptation leaflet positions and, thereby, reduce the amount of blood backflow required to seal the valve at the onset of each beat, thereby maximizing forward stroke volume and minimizing blood cell damage, as occurs during mechanical replacement valve closure, and *3*) provide a consistent and efficient LV outflow tract boundary surface geometry to funnel the blood flowing under the anterior leaflet toward the aortic valve during systolic ejection.

Implications. The results reported here provide a basis for a permanent paradigm shift from viewing the leaflets as passive flaps to viewing the leaflets as active, potentially adaptive, neurally controlled tissues whose complex function and dysfunction must be taken into account when considering not only therapeutic approaches to MV disease, but even the definitions of MV disease itself. The improved understanding of the structure-function relationships in these native, active valves could uncover new targets for pharmacological intervention and provide important insights to improve the future design and durability of tissue-engineered MVs.

The present study also employs the most sophisticated inverse finite-element model of the MV developed to date, inasmuch as it is based, for the first time, on experimental measurements of instantaneous LVP, LAP, and AoP with the simultaneous three-dimensional positions of all the elements of the mitral complex (annulus, leaflets, and papillary muscles) throughout the cardiac cycle in the beating heart. Such a finite-element model could find potential future applications as an aid to planning patient-specific medical and surgical therapies for MV disease, taking into account stress-and-strain distributions in the valve leaflets, as well as the location and function of critical blood vessels, nerves, and multiple, neurally controlled contractile systems.

ACKNOWLEDGMENTS

We thank David Liang for echocardiographic expertise and Koji Arata for acting as perfusionist in this study. We also thank Tom Nguyen for early planning contributions, Paul A. Chang and Eleazar P. Briones for technical assistance, Maggie Brophy and Sigurd Hartnett for careful marker image digitization, and George T. Daughters for extraction of four-dimensional data from marker coordinates.

GRANTS

This work was supported in part by National Heart, Lung, and Blood Institute Grants R01 HL-29589 and R01 HL-67025, Deutsche Herzstiftung (Frankfurt, Germany) Research Grant S/06/07 to W. Bothe, a fellowship from the Western States Affiliate of the American Heart Association to J. C. Swanson, and a Stanford Bio-X Graduate Student Fellowship to G. Krishnamurthy.

REFERENCES

1. **Ahmed A, Johansson O, Folan-Curran J.** Distribution of PGP 95, TH, NPY, SP and CGRP immunoreactive nerves in the rat and guinea pig atrioventricular valves and chordae tendineae. *J Anat* 191: 547–560, 1997.
2. **Boucek RJ, Bouckova B, Levy S.** Anatomical arrangement of muscle tissue in the anterior mitral leaflet in man. *Cardiovasc Res* 12: 675–680, 1978.
3. **Chen L, Yin FC, May-Newman K.** The structure and mechanical properties of the mitral valve leaflet-strut chordae transition zone. *J Biomech Eng* 126: 244–251, 2004.
4. **Chester AH, Taylor PM.** Molecular and functional characteristics of heart-valve interstitial cells. *Philos Trans R Soc Lond B Biol Sci* 362: 1437–1443, 2007.
5. **Cochran RP, Kunzelman KS, Chuong CJ, Sacks MS, Eberhart RC.** Nondestructive analysis of mitral valve collagen fiber orientation. *ASAIO Trans* 37: M447–M448, 1991.
6. **Cooper T, Napolitano L, Fitzgerald M, Moore K, Daggett W, Willman V, Sonnenblick E, Hanlon C.** Structural basis for cardiac valvular function. *Arch Surg* 93: 767–771, 1966.
7. **Curtis MB, Priola DV.** Mechanical properties of the canine mitral valve: effects of autonomic stimulation. *Am J Physiol Heart Circ Physiol* 262: H56–H62, 1992.
8. **De Biasi S, Vitellaro-Zuccarello L, Blum I.** Histochemical and ultrastructural study on the innervation of human and porcine atrio-ventricular valves. *Anat Embryol (Berl)* 169: 159–165, 1984.
9. **Ehinger B, Falck B, Persson H, Sporrong B.** Adrenergic and cholinesterase-containing neurons of the heart. *Histochemie* 16: 197–205, 1968.
10. **Ehinger B, Falck B, Stenevi U.** Adrenergic and non-adrenergic valvular nerves of the heart. *Experientia* 25: 742–743, 1969.
11. **Ellison JP, Hibbs RG.** The atrioventricular valves of the guinea-pig. I. A light microscopic study. *Am J Anat* 138: 331–345, 1973.

12. **Fenoglio J Jr, Tuan DP, Wit AL, Bassett AL, Wagner BM.** Canine mitral complex ultrastructure and electromechanical properties. *Circ Res* 31: 417–430, 1972.
13. **Filip DA, Radu A, Simionescu M.** Interstitial cells of the heart valves possess characteristics similar to smooth muscle cells. *Circ Res* 59: 310–320, 1986.
14. **Grande-Allen KJ, Barber JE, Klatka KM, Houghtaling PL, Vesely I, Moravec CS, McCarthy PM.** Mitral valve stiffening in end-stage heart failure: evidence of an organic contribution to functional mitral regurgitation. *J Thorac Cardiovasc Surg* 130: 783–790, 2005.
15. **Hadian M, Corcoran BM, Han RI, Grossmann JG, Bradshaw JP.** Collagen organization in canine myxomatous mitral valve disease: an x-ray diffraction study. *Biophys J* 93: 2472–2476, 2007.
16. **Herlihy JT, Murphy RA.** Force-velocity and series elastic characteristics of smooth muscle from the hog carotid artery. *Circ Res* 34: 461–466, 1974.
17. **Herlihy JT, Murphy RA.** Length-tension relationship of smooth muscle of the hog carotid artery. *Circ Res* 33: 275–283, 1973.
18. **Hibbs RG, Ellison JP.** The atrioventricular valves of the guinea-pig. II. An ultrastructural study. *Am J Anat* 138: 347–369, 1973.
19. **Jew JY, Fink CA, Williams TH.** Tyrosine hydroxylase- and nitric oxide synthase-immunoreactive nerve fibers in mitral valve of young adult and aged Fischer 344 rats. *J Auton Nerv Syst* 58: 35–43, 1996.
20. **Kawano H, Kawai S, Shirai T, Okada R.** Morphological study on vagal innervation in human atrioventricular valves using histochemical method. *Jpn Circ J* 57: 753–759, 1993.
21. **Krishnamurthy G, Ennis DB, Itoh A, Bothe W, Swanson JC, Karlsson M, Kuhl E, Miller DC, Ingels NB Jr.** Material properties of the ovine mitral valve anterior leaflet in vivo from inverse finite element analysis. *Am J Physiol Heart Circ Physiol* 295: H1141–H1149, 2008.
22. **Kunzelman KS, Cochran RP.** Stress/strain characteristics of porcine mitral valve tissue: parallel versus perpendicular collagen orientation. *J Card Surg* 7: 71–78, 1992.
23. **Latif N, Sarathchandra P, Taylor PM, Antoniw J, Yacoub MH.** Localization and pattern of expression of extracellular matrix components in human heart valves. *J Heart Valve Dis* 14: 218–227, 2005.
24. **Lushka H.** Das endocardium und die endocarditis. *Virchows Arch Path Anat* 4: 171–191, 1851.
25. **Maier LS, Barckhausen P, Weisser J, Aleksic I, Baryalei M, Pieske B.** Ca^{2+} handling in isolated human atrial myocardium. *Am J Physiol Heart Circ Physiol* 279: H952–H958, 2000.
26. **Marron K, Yacoub MH, Polak JM, Sheppard MN, Fagan D, Whitehead BF, de Leval MR, Anderson RH, Wharton J.** Innervation of human atrioventricular and arterial valves. *Circulation* 94: 368–375, 1996.
27. **May-Newman K, Yin FC.** Biaxial mechanical behavior of excised porcine mitral valve leaflets. *Am J Physiol Heart Circ Physiol* 269: H1319–H1327, 1995.
28. **Merryman WD, Youn I, Lukoff HD, Krueger PM, Guilak F, Hopkins RA, Sacks MS.** Correlation between heart valve interstitial cell stiffness and transvalvular pressure: implications for collagen biosynthesis. *Am J Physiol Heart Circ Physiol* 290: H224–H231, 2006.
29. **Miller MR, Kasahara M.** Studies on the nerve endings in the heart. *Am J Anat* 115: 217–233, 1964.
30. **Montiel MM.** Muscular apparatus of the mitral valve in man and its involvement in left-sided cardiac hypertrophy. *Am J Cardiol* 26: 341–344, 1970.
31. **Nicolai GF.** Die Mechanik des Kreislaufs. In: *Handbuch der Physiologie des Menschen*, edited by W Nagel. Braunschweig: Vieweg, 1909, p. 845–848.
32. **Priola DV, Fellows C, Moorehouse J, Sanchez R.** Mechanical activity of canine mitral valve in situ. *Am J Physiol* 219: 1647–1651, 1970.
33. **Priola DV, Fulton RL, Napolitano LM, Cooper T.** Electrical activity of the canine mitral valve in situ. *Am J Physiol* 216: 238–243, 1969.
34. **Reid A.** Heart. In: *Todd's Cyclopedia of Anatomy and Physiology*. London, 1839.
35. **Smirnow A.** Ueber die sensiblen Nervenendigungen im Hertzen bei Amphibien und Saeugetieren. *Anat Anz* 10: 737–749, 1895.
36. **Smith RB.** Intrinsic innervation of the atrioventricular and semilunar valves in various mammals. *J Anat* 108: 115–121, 1971.
37. **Smith RB, Taylor IM.** Atrioventricular and semilunar valve vascularization in rabbits and guinea pigs. *Acta Anat (Basel)* 78: 1–8, 1971.
38. **Smith S, Taylor PM, Chester AH, Allen SP, Dreger SA, Eastwood M, Yacoub MH.** Force generation of different human cardiac valve interstitial cells: relevance to individual valve function and tissue engineering. *J Heart Valve Dis* 16: 440–446, 2007.
39. **Sonnenblick EH, Napolitano LM, Daggett WM, Cooper T.** An intrinsic neuromuscular basis for mitral valve motion in the dog. *Circ Res* 21: 9–15, 1967.
40. **Taylor PM, Batten P, Brand NJ, Thomas PS, Yacoub MH.** The cardiac valve interstitial cell. *Int J Biochem Cell Biol* 35: 113–118, 2003.
41. **Timek TA, Lai DT, Dagum P, Tibayan F, Daughters GT, Liang D, Berry GJ, Miller DC, Ingels NB Jr.** Ablation of mitral annular and leaflet muscle: effects on annular and leaflet dynamics. *Am J Physiol Heart Circ Physiol* 285: H1668–H1674, 2003.
42. **Tsumori T, Domoto T.** Ultrastructural evidence for innervation of the endothelium and interstitial cells in the atrioventricular valves of the Japanese monkey. *Anat Rec* 240: 157–166, 1994.
43. **Williams TH.** Fast-conducting fibres in the mitral valve. *Br Heart J* 26: 554–557, 1964.
44. **Williams TH.** Mitral and tricuspid valve innervation. *Br Heart J* 26: 105–115, 1964.
45. **Williams TH, Folan JC, Jew JY, Wang YF.** Variations in atrioventricular valve innervation in four species of mammals. *Am J Anat* 187: 193–200, 1990.
46. **Williams TH, Jew JY.** Is the mitral valve passive flap theory overstated? An active valve is hypothesized. *Med Hypotheses* 62: 605–611, 2004.
47. **Wit AL, Fenoglio J Jr, Hordof AJ, Reemtsma K.** Ultrastructure and transmembrane potentials of cardiac muscle in the human anterior mitral valve leaflet. *Circulation* 59: 1284–1292, 1979.
48. **Wit AL, Fenoglio J Jr, Wagner BM, Bassett AL.** Electrophysiological properties of cardiac muscle in the anterior mitral valve leaflet and the adjacent atrium in the dog. Possible implications for the genesis of atrial dysrhythmias. *Circ Res* 32: 731–745, 1973.
49. **Wollard HH.** The innervation of the heart. *J Anat* 60: 345–373, 1926.
50. **Yin FC, Fung YC.** Mechanical properties of isolated mammalian ureteral segments. *Am J Physiol* 221: 1484–1493, 1971.